The infrared spectrum of XeH^+

S. A. Rogers, C. R. Brazier, and P. F. Bernath
Department of Chemistry, University of Arizona, Tucson, Arizona 85721

(Received 5 March 1987; accepted 17 March 1987)

The Fourier transform emission spectrum of XeH^+ was observed in the infrared region of the spectrum. The 1–0 and 2–1 vibration–rotation bands for $^{132}XeH^+$, $^{131}XeH^+$, and $^{129}XeH^+$ were recorded from a nickel hollow cathode discharge in xenon and hydrogen. Molecular constants, including $R_e = 1.602\,813(6)$ Å, $B_e = 6.560\,686(50)$, $\alpha_e = 0.186\,739(14)$, $\omega_e = 2269.9674(11)$, and $\omega_e x_e = 41.328\,30(34)$ cm^{-1} for $^{132}XeH^+$, were extracted from the line positions. Our work represents the first high-resolution detection of XeH^+.

I. INTRODUCTION

The protonated rare gases HeH^+, NeH^+, ArH^+, KrH^+, and XeH^+ form an unusual family of molecular ions. The high-resolution vibration–rotation transitions of HeH^+,[1,2] NeH^+,[3,4] ArH^+,[5,6] and KrH^+ [6] have been previously observed. A complete set of references to the high-resolution work on these ions is provided in a recent NeH^+ paper[4] and will not be repeated here. Most recently, the dipole moment of ArH^+ was estimated from a determination of the g values of ArD^+ and ArH^+ by detection of the pure rotational transitions in a magnetic field.[7] We report here on the vibration–rotation spectrum of XeH^+. XeH^+ is the simplest Xe containing molecule. The observation of XeH^+ completes the protonated rare gas series unless there are experimentalists willing to tackle RnH^+.

The best theoretical predictions for the molecular properties of XeH^+ are by Klein and Rosmus.[9] The quantum chemical calculations of Rosmus and co-workers on NeH^+,[10] ArH^+,[11] KrH^+,[10] and, now, XeH^+ are in excellent agreement with the experimental observations.

II. EXPERIMENTAL

The XeH^+ spectra were generated in a water-cooled nickel hollow cathode discharge lamp at a current of 200 mA. A slow, continuous flow 2.2 Torr of H_2 and 100 mTorr of Xe was maintained through the lamp.

The spectrum was recorded with the Fourier transform spectrometer associated with the McMath Solar Telescope of the National Solar Observatory at Kitt Peak. The 1800–5000 cm^{-1} region of the spectrum was recorded at 0.020 cm^{-1} resolution using liquid nitrogen-cooled InSb detectors and a wedged Ge filter. The lower wave number limit was determined by the red limit of the detector, while the upper limit was set by the Ge filter. Twenty scans were co-added in $1\frac{1}{2}$ hours of integration. The interferogram was Fourier transformed into a spectrum by G. Ladd of the National Solar Observatory.

III. RESULTS

The presence of the 1–0 band of XeH^+ was first indicated by the observation of the characteristic isotopic pattern of Xe. Xe has nine stable isotopes: $^{124}Xe(0.1\%)$, $^{126}Xe(0.1\%)$, $^{128}Xe(1.9\%)$, $^{129}Xe(26.4\%)$, $^{130}Xe(4.1\%)$, $^{131}Xe(21.2\%)$, $^{132}Xe(26.9\%)$, $^{134}Xe(10.4\%)$, and $^{136}Xe(8.9\%)$. The three most abundant isotopes, ^{132}Xe, ^{131}Xe, and ^{129}Xe provide a triplet pattern when the signal-to-noise ratio is small and the ^{134}Xe and ^{136}Xe isotopomers can also be seen weakly (Fig. 1). It was possible to pick out $R(16)$ to $P(18)$ in the fundamental band. The theoretical $\omega_e x_e$ (41.2 cm^{-1}) allowed the 2–1 band to be predicted and found, but the 3–2 and 2–0 bands were too weak to be detected. The observed line position for the 1–0 and 2–1 vibration–rotation bands of $^{132}XeH^+$, $^{131}XeH^+$, and $^{129}XeH^+$ are provided in Table I. Although the transitions for some of the other isotopes could be picked out for the strongest lines, it was decided to analyze only these three main isotopes.

The line positions of Table I were determined with the aid of a Kitt Peak data reduction program called DECOMP. Voigt line shape functions were fitted to the lines by a nonlinear least-squares procedure. The observed linewidths of 0.020 cm^{-1} (full width at half-maximum) were set by the spectrometer resolution (0.02 cm^{-1}) rather than by Doppler or pressure broadening. The largest signal-to-noise ratio observed was about 10 (Fig. 1), so the precision of the best lines in Table I is $0.02/10 = 0.002$ cm^{-1}. The absolute calibration of $\pm$ 0.001 cm^{-1} was accomplished by observa-

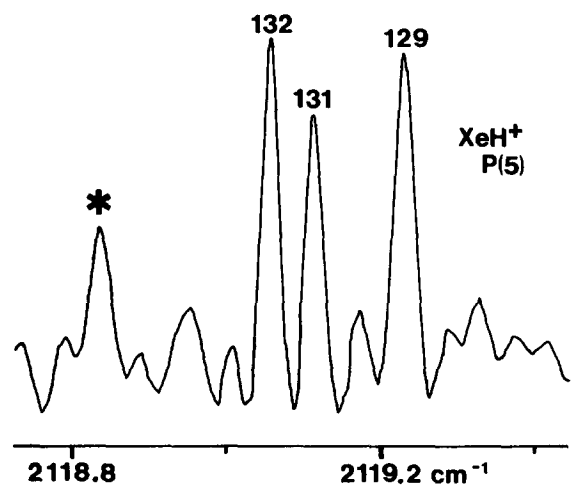

FIG. 1. The $P(5)$ vibration–rotation emission line of XeH^+ in the fundamental 1–0 band. The numerical labels refer to the $^{132}XeH^+$, $^{131}XeH^+$, and $^{129}XeH^+$ isotopic forms of XeH^+. There is some evidence for the appearance of two of the less abundant isotopic species. The feature marked by an asterisk is due to $^{136}XeH^+$, while the $^{134}XeH^+$ peak lines between the $^{136}XeH^+$ peak and the peak labeled 132. For most transitions, only the three strongest isotopic lines were observed.

 0021-9606/87/130159-04$02.10

TABLE I. The observed line positions for the vibration–rotation spectrum of XeH^+ (in cm^{-1}) [the numbers in parentheses are observed − calculated line positions using the constants of Table II (in 10^{-4} cm^{-1})].

	(1,0)		(2,1)	
J	$R(J)$	$P(J)$	$R(J)$	$P(J)$
0	2199.8930(31)[a]		2116.8804(9)	
	2199.9457(− 32)		2116.9290(− 57)	
	2200.0821(37)		2117.0566(33)	
1	2212.0728(− 39)	2174.3914(− 13)	2128.6980(− 15)	...
	2212.1384(22)	2174.4489(− 17)	2128.7666(110)	...
	2212.2598(− 72)	2174.5790(22)	2128.8734(− 19)	...
2	2223.8828(8)	2161.0915(− 11)	2140.1403(0)	2079.1866(− 88)
	2223.9449(29)	2161.1495(− 6)	2140.2029(55)	2079.2586(95)
	2224.0740(0)	2161.2773(30)	2140.3172(− 8)	2079.3674(44)
3	2235.2996(− 10)	2147.4329(9)	2151.1976(10)	2065.9060(− 42)
	2235.3603(− 8)	2147.4918(28)	2151.2613(64)	2065.9600(− 37)
	2235.4908(− 34)	2147.6118(7)	2151.3756(− 6)	2066.0762(6)
4	2246.3287(14)	2133.4156(− 5)	2161.8631(− 4)	2052.2713(− 4)
	2246.3877(− 8)	2133.4715(− 11)	2161.9216(− 13)	2052.3255(3)
	2246.5219(− 5)	2133.5928(4)	2162.0448(0)	2052.4333(− 15)
5	2256.9571(− 1)	2119.0512(10)	2172.1368(8)	2038.2956(102)
	2257.0163(− 26)	2119.1071(9)	2172.1931(− 34)	2038.3373(− 17)
	2257.1534(− 2)	2119.2241(5)	2172.3205(17)	2038.4449(− 13)
6	2267.1857(6)	2104.3402(5)	2182.0074(− 16)	2023.9616(51)
	2267.2472(− 3)	2104.3985(33)	2182.0699(− 5)	2024.0086(− 16)
	2267.3824(− 4)	2104.5111(11)	2182.1952(20)	2024.1107(− 41)
7	2277.0075(14)	2089.2892(− 6)	b	2009.2927(22)
	2277.0689(− 1)	2089.3464(16)	2191.5412(15)	2009.3447(5)
	2277.2054(6)	2089.4571(0)	2191.6671(42)	2009.4424(− 37)
8	2286.4146(− 4)	2073.9070(10)	2200.5393(24)	1994.2929(2)
	2286.4731(− 55)	2073.9620(15)	2200.6006(12)	1994.3432(− 30)
	2286.6155(6)	2074.0709(9)	2200.7231(1)	1994.4440(− 14)
9	2295.4060(− 10)	2058.1944(8)	2209.1775(− 46)	1978.9653(− 33)
	2295.4721(9)	2058.2492(17)	2209.2468(24)	1979.0199(− 18)
	2295.6043(− 37)	2058.3549(5)	2209.3666(− 20)	1979.1196(16)
10	2303.9773(1)	2042.1562(− 19)	2217.4069(− 14)	1963.3246(11)
	2304.0412(− 8)	2042.2129(16)	2217.4583(− 116)	1963.3758(1)
	b	2042.3146(− 10)	2217.5915(− 33)	1963.4688(− 5)
11	2312.1206(− 1)	2025.8028(− 19)	2225.2143(33)	1947.3659(30)
	2312.1833(− 28)	2025.8559(− 13)	2225.2695(− 13)	1947.4115(− 22)
	2312.3257(16)	2025.9610(20)	2225.3973(5)	1947.5035(− 13)
12	2319.8372(45)	2009.1380(− 9)	2232.5802(− 52)	
	2319.9025(39)	2009.1906(0)	2232.6474(50)	
	2320.0366(− 9)	2009.2927(27)	2232.7732(33)	
13	2327.1106(22)	1992.1628(− 33)	2239.5282(14)	
	2327.1702(− 47)	1992.2157(− 13)	2239.5792(− 7)	
	2327.3123(− 25)	1992.3126(− 16)	2239.7150(57)	
14	c	1974.8935(19)	2246.0318(10)	
	c	1974.9426(11)	2246.0767(− 17)	
	c	1975.0373(4)	2246.2053(− 51)	
15	2340.3299(− 24)	1957.3224(14)		
	2340.4009(13)	1957.3717(19)		
	2340.5442(16)	1957.4631(− 5)		
16	2346.2668(− 44)	1939.4582(− 14)		
	2346.3497(109)	1939.5091(20)		
	2346.4784(− 56)	1939.5986(− 12)		
17		1921.3118(− 10)		
		1921.3561(− 28)		
		1921.4523(13)		
18		1902.8875(16)		
		1902.9353(49)		
		1903.0143(− 83)		

[a] The upper (middle, lower) number for each J corresponds to the ^{132}Xe (^{131}Xe, ^{129}Xe) isotope.
[b] Obscured by an atomic line.
[c] Overlapped by CO_2 absorption.

tion of the vibration–rotation lines of the impurity OH.[12] Although the XeH^+ vibration–rotation lines are very weak, much stronger lines attributed to infrared electronic transitions of the Rydberg molecule XeH were also present.[13] These results will be reported elsewhere.[14]

The lines of Table I were reduced to molecular constants (Tables II and III) in two ways. All of the line positions in Table I (1–0 and 2–1 bands for three isotopomers) were fit

TABLE II. Molecular constants for the ground state of XeH^+ (in cm^{-1}).

Molecular constants[a]	$v=0$	$v=1$	$v=2$
T_v	0.0[b]	2187.326 9(8)	4292.012 2(13)
	0.0	2187.385 3(8)	4292.125 1(15)
	0.0	2187.513 2(8)	4292.370 3(12)
B_v	6.467 430(41)	6.281 979(43)	6.097 506(49)
	6.467 776(42)	6.282 233(43)	6.097 856(48)
	6.468 657(42)	6.283 018(43)	6.098 524(46)
$10^3 \times D_v$	0.218 59(12)	0.217 52(14)	0.216 06(16)
	0.218 45(13)	0.217 43(14)	0.216 64(17)
	0.218 65(12)	0.217 41(14)	0.216 30(16)

[a] The values in parentheses represent one standard deviation in the last digit. H_v is fixed to 2.67×10^{-9} for all isotopes in all vibrational levels (see the text).

[b] The upper (middle, lower) number for each constant corresponds to the ^{132}Xe (^{131}Xe,^{129}Xe) isotope.

with the mass-reduced Dunham expression[15]:

$$E_{v,J} = \sum_{k,l} \mu^{-(k/2+l)} U_{kl} (v+\tfrac{1}{2})^k [J(J+1)]^l,$$

where μ is the charge-adjusted reduced mass.[15] The U_{kl} constants of this fit are provided in Table III, as are the conventional Dunham[16] Y_{kl}'s for $^{132}XeH^+$:

$$E_{v,J} = \sum_{k,l} Y_{kl} (v+\tfrac{1}{2})^k [J(J+1)]^l.$$

Note that no Watson Δ parameters,[15] which account for the breakdown of the Born–Oppenheimer approximation, were required for this fit. The standard deviation of the fit was 0.0034 cm^{-1}, in good agreement with the expected average precision of the data.

A "conventional" simultaneous fit of the 1–0 and 2–1 bands for each separate isotope produces the spectroscopic constants of Table II. The required nine H parameters could not be simultaneously determined, so they were fixed to the value obtained in the Dunham fit (Table III). The standard deviation of the conventional fit and the mass-reduced Dunham fit were essentially the same.

The constants of Table III are equilibrium molecular constants so $Y_{10} = \omega_e = 2269.9674(11)$ cm^{-1}, $-Y_{20} = \omega_e x_e = 41.320\,56(34)$ cm^{-1}, $Y_{01} = B_e = 6.560\,686(50)$, $-Y_{11} = \alpha_e = 0.186\,686(14)$ cm^{-1}, etc. The statistical errors in Table III do not include the substantial systematic errors present due to the neglect of higher order terms such as $Y_{30} = \omega_e y_e$. The $G(v)$ (ω_e,$\omega_e x_e$), $B(v)$ (B_e,α_e,γ_e) constants and the charge-adjusted reduced mass[14] were used as input to an RKR program to provide the turning points of the potential curve (Table IV). The turning points of Table IV for $v > 2$ are extrapolations and should be used with great caution. The $G(v)$ and $B(v)$ polynomials used to generate the potential curve are not very reliable predictors of unknown vibrational and rotational constants for diatomic hydrides.

The U_{01} value of Table III was used to compute the equilibrium internuclear separation of 1.602 813(6) Å from the equation $U_{01}(R_e^{BO})^2 = 505\,379$ MHz Å^2 amu.[17]

TABLE III. Dunham coefficients for the ground state of XeH^+ (U's are in cm^{-1} $amu^{(k/2+l)}$ and Y's are in cm^{-1}).

k	l	U_{kl}	Y_{kl}
1	0	2270.179 9(11)[a]	2269.967 4[b]
2	0	−41.328 30(34)	−41.320 56
0	1	6.561 914(50)[c]	6.560 686
1	1	−0.186 739(14)	−0.186 686
2	1	$0.565\,4(35) \times 10^{-3}$	$0.565\,1 \times 10^{-3}$
0	2	$-0.219\,15(34) \times 10^{-3}$	$-0.219\,07 \times 10^{-3}$
1	2	$0.110\,8(37) \times 10^{-5}$	$0.110\,8 \times 10^{-5}$
0	3	$0.267(67) \times 10^{-8}$	0.267×10^{-8}

[a] The errors quoted in parentheses are one standard deviation in the last digit.

[b] The listed Y_{kl} values are for $^{132}XeH^+$.

[c] The value of $R_e = 1.602\,81(6)$ Å from U_{01} and the conversion factor in Ref. 16.

IV. DISCUSSION

The *ab initio* calculation by Klein and Rosmus[9] was helpful in identifying XeH^+. In Table V the experimental and *ab initio* theoretical predictions of the molecular constants of NeH^+, ArH^+, KrH^+, and XeH^+ are given. HeH^+ is excluded from Table V because the experimental measurements are not extensive enough to provide equilibrium molecular constants. The largest deviation in R_e is 0.008 Å for XeH^+, while ω_e is off by 66 cm^{-1} for KrH^+. While the quantum chemical calculations were not an absolutely vital aid to the experimentalists, they were very helpful in narrowing the search windows and confirming the identification of the protonated rare gases.

The calculation of the vibration–rotation transition dipole moments (and the equivalent Einstein A factors) of the protonated rare gases by Klein and Rosmus[9] explains our relatively poor signal-to-noise ratio. The XeH^+ molecule has the smallest dipole moment (1.55 D), the smallest dipole moment derivative (2.16 D/Å), and the smallest vibration frequency ($\omega_e = 2270$ cm^{-1}) of all the protonated rare gases.[9] This results in an Einstein A value of 125 s^{-1} (a transition dipole moment of 0.189 D) for $v = 1 \rightarrow v = 0$ which is more than a factor of 2 smaller than any other protonated rare gas ($A = 285$ s^{-1} for KrH^+).[9] Furthermore, the many Xe isotopes reduce the intensity of any given vibration–rotation line by at least a factor of 4.

The chemistry of xenon in a hydrogen discharge is also different from the other rare gases. Xe has a proton affinity

TABLE IV. RKR turning points for the $X\,^1\Sigma^+$ state of $^{132}XeH^+$.

v	E_v (cm^{-1})	R_{min} (Å)	R_{max} (Å)
0	1125.7626	1.492 28	1.738 00
0.5	2229.7559	1.452 60	1.802 71
1.0	3313.0889	1.424 28	1.856 44
1.5	4375.7616	1.401 77	1.904 79
2.0	5417.7741	1.382 90	1.949 90
2.5	6439.1262	1.366 60	1.992 89
3.0	7439.8181	1.352 21	2.034 42
3.5	8419.8497	1.339 31	2.074 92
4.0	9379.2210	1.327 61	2.114 73

TABLE V. A comparison of the experimental and *ab initio* theoretical molecular constants of the protonated rare gases.

Molecule		R_e (Å)	B_e (cm^{-1})	α_e (cm^{-1})	ω_e (cm^{-1})	$\omega_e x_e$ (cm^{-1})
$^{20}NeH^+$	expt.[a]	0.991 195(21)	17.884 72(75)	1.096 78(27)	2903.751(23)	113.358 1(74)
	calc.[b]	0.996	17.72	1.096	2896	113
$^{40}ArH^+$	expt.[c]	1.280 372 6(1)	10.461 269(18)	0.378 774(11)	2710.9199(56)	61.637 7(35)
	calc.[d]	1.286	10.36	0.364	2723	56
$^{84}KrH^+$	expt.[c]	1.421 191 1(7)	8.381 451(10)	0.2670 704(25)	2494.653 81(34)	48.529 38(13)
	calc.[b]	1.419	8.41	0.256	2561	49
$^{132}XeH^+$	expt.[e]	1.602 813(6)	6.560 686(50)	0.186 686(14)	2269.967 4(11)	41.320 56(34)
	calc.[f]	1.611	6.49	0.180	2313.6	41.2

[a] Reference 4.
[b] Reference 10.
[c] Reference 6.
[d] Reference 11.
[e] This work.
[f] Reference 9.

of 118 kcal/mol,[18] which is larger than the proton affinity of H_2 (104 kcal/mol).[18] This means that H_3^+, the dominant ion in a hydrogen discharge, will transfer a proton to Xe to make XeH^+. Unlike the other protonated rare gases, an excess of H_2 provides the most favorable conditions for XeH^+ production. Indeed, when we discharged 1.2 Torr of Xe and 0.02 Torr of H_2, no XeH^+ was detected. The other rare gases have proton affinities less than that of H_2, except Kr, which has a proton affinity almost identical with the value for H_2.[18]

The XeH^+ molecule dissociates to Xe^+ and H with a calculated D_0 of 3.90 eV (90 kcal/mol).[9] The other protonated rare gases dissociate to the rare gas neutral and the H^+ ion. This happens because only for Xe is the ionization potential (97 834 cm^{-1}) of the rare gas less than the ionization potential of H (109 678 cm^{-1}).[19] Like the other protonated rare gases, the charge distribution is approximately H^+–Rg (Rg = rare gas) near the equilibrium internuclear separation but, unlike the others, an avoided curve crossing occurs at long range as the charge distribution shifts to H–Xe^+ near dissociation.[9]

ACKNOWLEDGMENTS

We thank Jeremy Wagner for expert technical assistance at Kitt Peak. We also thank John Johns for providing us with a copy of his Dunham fitting program. Acknowledgement is made to the Donors of the Petroleum Research Fund, administered by the American Chemical Society, for support of this research. The National Solar Observatory is operated by the Association for Research in Astronomy, Inc., under contract with the National Science Foundation.

[1] P. Bernath and T. Amano, Phys. Rev. Lett. **48**, 20 (1982).
[2] D. E. Toliver, G. A. Kyrala, and W. H. Wing, Phys. Rev. Lett. **43**, 1719 (1979).
[3] M. Wong, P. Bernath, and T. Amano, J. Chem. Phys. **77**, 693 (1982).
[4] R. S. Ram, P. F. Bernath, and J. W. Brault, J. Mol. Spectrosc. **113**, 451 (1985).
[5] J. W. Brault and S. P. Davis, Phys. Scr. **25**, 268 (1982).
[6] J. W. C. Johns, J. Mol. Spectrosc. **106**, 124 (1984).
[7] K. B. Laughlin, G. A. Blake, R. C. Cohen, and R. J. Saykally, Phys. Rev. Lett. **58**, 996 (1987).
[8] H. P. Weise, H. U. Mittmann, A. Ding, and A. Henglein, Z. Naturforsch. Teil A **26**, 1122 (1971).
[9] R. Klein and P. Rosmus, Z. Naturforsch. Teil A **39**, 349 (1984).
[10] P. Rosmus and E. A. Reinsch, Z. Naturforsch. Teil A **35**, 1066 (1980).
[11] P. Rosmus, Theor. Chim. Acta **51**, 359 (1979).
[12] T. Amano, J. Mol. Spectrosc. **103**, 436 (1984).
[13] R. Lipson, Chem. Phys. Lett. **129**, 82 (1986); (private communication).
[14] M. H. Douay, S. A. Rogers, and P. F. Bernath (work in progress).
[15] J. K. G. Watson, J. Mol. Spectrosc. **80**, 411 (1980).
[16] J. L. Dunham, Phys. Rev. **41**, 721 (1932).
[17] M. Bogey, C. Demuynck, and J. L. Destombes, J. Chem. Phys. **79**, 4704 (1983).
[18] D. K. Bohme, G. I. Mackay, and H. I. Schiff, J. Chem. Phys. **73**, 4976 (1980).
[19] C. E. Moore, *Ionization Potentials and Ionization Limits Derived from the Analyses of Optical Spectra*, Natl. Stand. Ref. Data Ser. Natl. Bur. Stand. 34(U. S. GPO, Washington, D.C., 1970).